Demonstration of femtosecond laser micromachining for figure correction of thin silicon optics for X-ray telescopes

Heng E. Zuo[a,c], Brandon D. Chalifoux[b], Ralf K. Heilmann[b], Sang-Hoon Nam[c], Kyung-Han Hong[c], and Mark L. Schattenburg[b]

[a]Department of Aeronautics & Astronautics, MIT, Cambridge, MA, 02139, USA
[b]Kavli Institute for Astrophysics and Space Research, MIT, Cambridge, MA, 02139, USA
[c]Research Laboratory of Electronics, MIT, Cambridge, MA, 02139, USA

ABSTRACT

Future space X-ray telescopes, for example, the Lynx X-ray Observatory under study in the 2020 Astrophysics Decadal Survey, require high angular resolution, large field of view and large effective area X-ray mirrors. Various scientific, engineering and economic considerations make the manufacturing of the telescope optics challenging. In spite of many major improvements in current methods, including slumping (glass shaping), silicon pore optics, and monocrystalline silicon polishing, etc., the required resolution and stability in thin optics have not yet been demonstrated. Furthermore, the high reflective coating films on the mirrors can stress and distort the mirror figure. Therefore, additional steps to correct the mirrors are needed to achieve the stringent requirements for the next generation high-performance X-ray mirrors. In this paper, we demonstrate a novel X-ray mirror figure correction method with the use of femtosecond lasers.

Over the last two decades, rapid developments of ultrafast laser technologies have triggered wide applications in the processing of both transparent and opaque materials, from material micromachining to nano-surgeries. We apply this technology in a novel stress-based figure correction technique for X-ray telescope mirrors. We use femtosecond laser beams to micromachine thermal oxide layers on the back side of silicon mirrors, from which regions of intrinsic compressive stress are removed. We pattern laser micromachined spots over the full mirror to compensate the undesired stress introduced from mirror manufacturing processes and reflective coatings. We built a new optics setup using an infrared laser of 220 fs pulse duration and 1 kHz repetition rate, and we designed a procedure for imaging, correcting and measuring mirror substrates with this setup. In this paper, we present the experimental results on the stress manipulation in flat silicon substrates, showing the laser induced integrated stress increases almost linearly with the fraction of area removal in the micromachining. This indicates great potential for correcting thin silicon optics by using appropriate machining parameters for future X-ray telescopes.

Keywords: X-ray telescope, thin mirrors, figure correction, femtosecond laser, micromachining, thermal oxides

1. BACKGROUND

1.1 Requirements for future X-ray space telescopes

X-ray telescopes are launched to above the Earth's atmosphere to observe astronomical objects with high altitude rockets, balloons and satellites. Despite their current success in X-ray astronomy, future X-ray space telescopes need to meet more stringent requirements for high angular resolution, large field of view and large effective area[1] in order to study astrophysical phenomena in much finer detail. Besides these science goals, the economic and mass constraints require the telescopes to be equipped with thinner mirrors which can be made faster and cheaper. For instance, the NASA Lynx X-ray telescope mission concept, currently under study for consideration in the 2020 Decadal Review, has science goals of achieving an angular resolution of $0.5''$ (arcsecond), the same as NASA's Chandra X-ray Observatory, but with thirty times more collecting areas and a much wider field of

Further author information: (Send correspondence to Heng E. Zuo)
E-mail: zuoh@mit.edu, Telephone: 1 617 803 9960

Optics for EUV, X-Ray, and Gamma-Ray Astronomy IX, edited by Stephen L. O'Dell, Giovanni Pareschi, Proc. of SPIE Vol. 11119, 111191A · © 2019 SPIE · CCC code: 0277-786X/19/$21 · doi: 10.1117/12.2530947

view while still fitting inside the launch vehicle. Therefore Lynx needs to use light-weight mirrors forty times thinner than those on Chandra, while maintaining the high resolution.

Chandra's mirrors were made by grinding and polishing thick Zerodur shells, followed by coatings of highly reflective iridium metal. In spite of the great technical accomplishment, this method doesn't work well with very thin mirrors which may be distorted during the grinding process, and new ways of making mirrors need to be explored. Many different concepts for thin X-ray mirrors have been proposed in the last twenty years, including glass slumping,[2,3] full-shell X-ray optics,[4] silicon pore optics,[5] monocrystalline silicon polishing,[6,7] etc. Despite the improvements achieved by some of these methods over the past ten years, they are still limited in terms of approaching the half arc-second resolution goal. So additional steps to correct or compensate the error terms are critical to the successful making of the mirrors. Furthermore, if one correction pass is not enough to achieve a perfect mirror, multiple correction passes will be needed to remove residual unwanted shape errors.

The shape errors in X-ray mirrors that need to be corrected mainly come from two sources: the original shape errors from the mirror manufacturing process, and the stress-induced shape errors introduced by reflective coatings and mirror mounting procedures. The performance of X-ray mirrors, especially in the soft X-ray band ($0.1-10\,\mathrm{keV}$) depends not only on the surface quality but also on the reflective coatings. These coatings are dense and smooth films, typically composed of high-density elements such as gold or iridium, sputtered on top of the mirrors to increase the critical angle of reflection for X-rays as well as the reflectivity. The down side of these coatings, however, is that they typically exhibit high compressive stress, which can distort the mirror substrates severely from their designed shapes. Although there are some groups trying to create high quality and low stress iridium films, they report residual figure errors on coated mirrors of no less than $1''$.

Correction techniques	Ion beam figuring[8]	Piezo-electric film adjusting[9]	Ion implant[10]	Oxide patterning with photo-lithography[11]	Femtosecond laser micromachining
Pros	Standard and well-understood process; High spatial resolution	In-situ adjustment	Single process step; Stable with annealing	Standard industrial process; Inherently stable; Best accuracy demonstrated	Single and fast process step; Capable of multi-pass corrections; Complements other methods
Cons	Mid-range frequency errors	Complex processes with many steps; Stability has not been demonstrated	Large expensive machine; Vacuum environment	Complex processes with many steps; Strength has not been demonstrated	Stability and strength have not been demonstrated

Table 1: Comparison of X-ray telescope mirror correction techniques

Table 1 compares some of the correction techniques used or proposed by various groups in the past decade. The last three techniques are all developed at the MIT Space Nanotechnology Lab. Ion implantation is a single-step process which results in stable corrections of the mirrors, but it requires a large expensive ion generator and vacuum environment. The oxide patterning with photo-lithography and acid etching has produced the most accurate corrections so far, but the whole process includes more than ten steps, most of which need to be done in the clean room. To take advantages of the above two methods while avoiding some of the problems, we investigated a third approach — femtosecond laser micromachining, which is a fast process with a single step to create patterns in a thermal oxide layer at the back of the silicon mirrors to correct shape errors. The technology enabling this approach is briefly introduced in the next section. The primary goal of this work is to achieve good correction accuracy, comparable to oxide patterning with photo-lithography and acid etching, but with a much easier process.

1.2 Comparison of different laser processing techniques

Traditional laser processing typically uses laser sources that generate pulses with duration of nanoseconds (10^{-9} s) or longer, which leads to a series of thermal effects including a large heat-affected zone, and shock waves propagating towards surrounding areas where micro cracks form. The molten materials at the focus of the laser beams are ejected to the surface, forming a recast layer with debris and damages caused to adjacent structures. Results in less precise machining, which cannot be used to achieve the precision and surface quality required for X-ray mirrors.

On the other hand, ultrafast laser micromachining, which applies lasers of extremely short pulse duration — typically on the order of picosecond (10^{-12} s) and femtosecond (10^{-15} s) range — to remove materials or to change the properties of materials, is capable of producing high-precision machining with less collateral damage. During the last two decades, various research has been conducted with this type of technique, exploring practical applications.[12–14] Unlike laser processing with longer pulsewidths, which rely on photo-thermal interaction, ultrafast laser micromachining is essentially a non-thermal process,[15] where a large (10 % or more) number of valence electrons inside the laser-exposed regions are excited in a very short time,[16] leading to the formation of a hot dense ion electron plasma. The timescale of such photo-absorption is so short, that the energy deposited to the area of impact cannot be carried to the surrounding areas,[17] resulting in an inherently colder process leaving a cleaner hole with less recast material and a reduced heat-affected zone.

Because femtosecond laser micromachining is capable of creating micron-scale features with high surface quality and great dimensional accuracy,[18,19] while avoiding peripheral thermal damage to surrounding materials, it can deliver the performance, speed, and economy required to correct X-ray mirrors. The three-dimensional degree of freedom of the micromachining enables processing on curved surfaces,[20] and this provides a huge advantage over some other correction techniques. The material independence of absorption processes in certain materials enables fabrication in compound substrates composed of different materials,[15] which is an important aspect of the method that we propose to correct X-ray mirrors. The details are discussed in the next section.

2. METHODS

The next generation of high-performance X-ray mirrors will benefit from the excellent figure enabled by accurate correction, without affecting the high reflectivity provided by the coating films. To correct the figure errors and address the distortion induced by coating stress on silicon mirrors, we have developed a new process using femtosecond laser micromachining to create thermal oxide patterns on the backside of the mirrors.

2.1 Process flow of mirror correction with micromachining

Previous research using ultrafast lasers micro-stressing has corrected fused silica optics by directly modifying internal materials without using additional stress layers,[21] but that approach may not work for silicon mirrors because the stress induced in the silicon can be insufficient to correct figure errors. Therefore, we propose a new method for silicon mirrors with the aid of an additional thermal oxide stress layer. The process of stress-based silicon mirror correction using thermal oxide patterning on thin silicon mirrors consists of four steps, which are illustrated in Figure 1.

The process starts with a bare silicon mirror, which has figure errors to be corrected, manufactured using, for example, the monocrystalline silicon polishing method at NASA Goddard Space Flight Center. The first step is to expose the mirror to a combination of oxidizing agents and heat, to grow a layer of silicon dioxide (SiO_2) on both sides of the mirror. Research has shown the growth of thermal oxides on silicon to be repeatable and stable, leaving intrinsic compressive stress inside the oxide layer of around 300 MPa depending on the growth temperature and substrate orientation.[22,23] The integrated stress in this layer, which is the film stress integrated over its thickness, can be adjusted by varying the thickness based on the need.

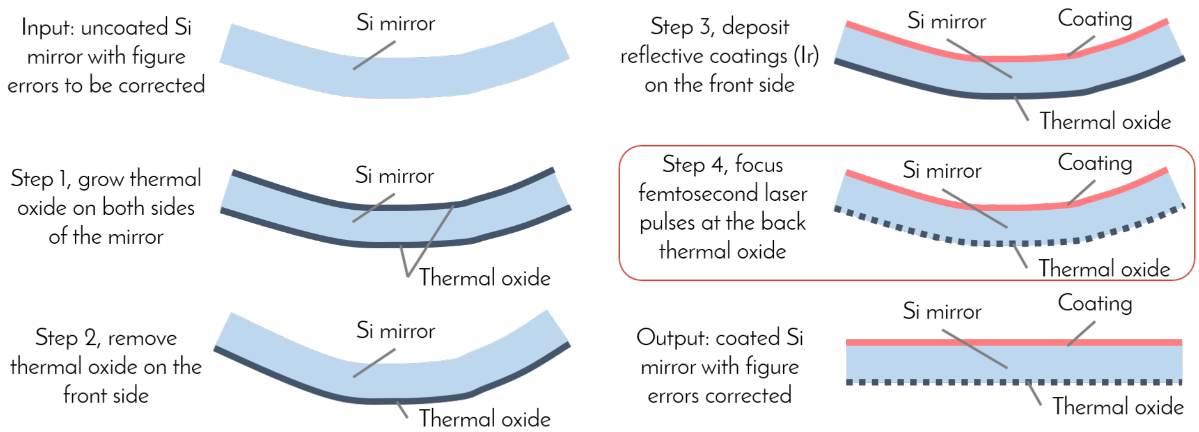

Figure 1: Process flow of stress-based silicon mirror correction using thermal oxide patterning on thin silicon mirrors. Step 4 (highlighted in red box) is the correction step with femtosecond laser micromachining.

After oxidation, the second step is to remove the thermal oxide film on the front side of the silicon mirror with buffered oxide etch. The back side oxide film is protected with photoresist, which is removed later by piranha solution. In the next step, the mirror is coated with high reflective coatings such as iridium using a sputtering system.[24] There could be some thermal annealing cycles needed to ensure the stability of the coating. Then the surface profile of the mirror's front side needs to be measured, which will be used to generate an error map to be corrected for. Up to this point, the whole process is quite similar to the process for stress compensation by thermal oxide patterning with photo-lithography,[11] but the difference is in the next step.

Step 4, highlighted in red box in Figure 1, is the correction step with femtosecond laser micromachining. Laser pulses are focused in the thermal oxide layer at the back side of the mirror substrate and holes in the 5 µm to 50 µm range are created. The removal of the stressed film inside these holes allows the materials in the adjacent regions to relax, which leads to stress relaxation and substrate bending to compensate for the figure errors. To achieve this stress compensation over the full mirror, the substrate needs to be moved relative to the laser beam to expose patterns across the whole substrate. An algorithm is used to determine the amount of material to be removed in different regions based on the error map from the previous step. By tuning the micromachining parameters locally in different regions, we can essentially achieve an accurate correction of the coated silicon mirror, which is the output of this whole process.

This correction technique has the advantage of high precision and controllability with minimized affected volume, like some of the other applications of femtosecond laser micromachining. It can provide the speed and adjustability that other correction techniques do not have, and it is capable of multi-pass corrections in case that single-pass correction is insufficient to cancel out all the unwanted error terms. These residual error terms may come from ray-trace errors in the measurements or handling errors due to insufficient process control, and the multi-pass corrections can function as a feedback loop to achieve higher accuracy. This approach can be adapted to curved mirrors, such as the hyperbolic and parabolic mirrors required for Wolter type X-ray telescopes, with a set-up that enables more degrees of motions of the mirror substrates.

2.2 Optics design and experiment set-up

To demonstrate Step 4 in the above process, we designed an optical system to test the micromachining of flat silicon wafers with thermal oxides on both sides. A femtosecond laser from IPG Photonics utilizes a Cr:ZnS laser seeded Cr:ZnSe chirped-pulse amplifier which provides $\tau = 220$ fs and 1.2 mJ pulses at the mid-IR wavelength of $\lambda = 2.4$ µm at 1 kHz repetition rate. The reason for using a mid-IR laser over a typical near-IR laser at 800 nm or 1030 nm is to decrease the linear absorption of light in the silicon substrate, in order to create deeper holes into the mirror to enhance the effects of stress relaxation. The laser beam is linearly polarized and the pulse energy is attenuated down to as low as 1 µJ, providing sufficient energy for micromachining.

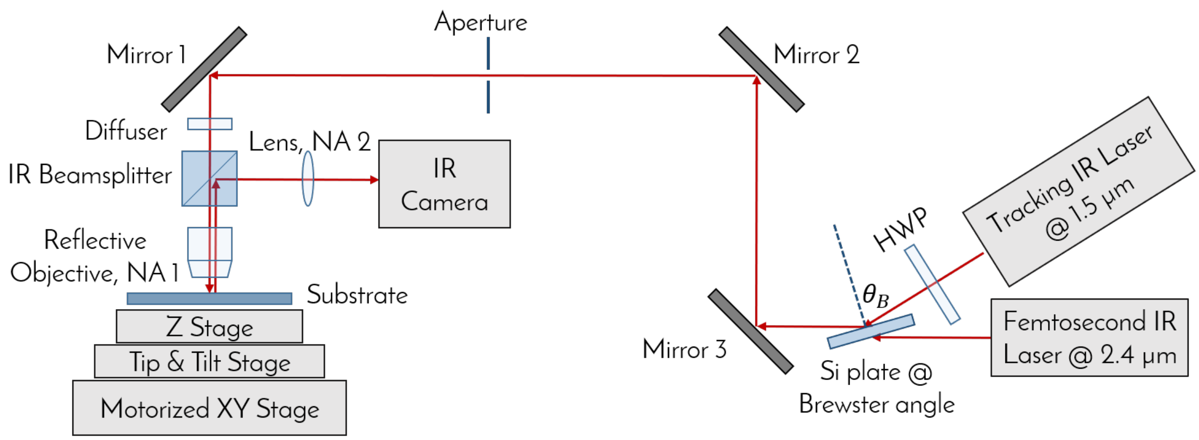

Figure 2: Optics design for micromachining flat silicon wafers with mid-IR femtosecond laser (front side view).

The optical design is illustrated in Figure 2. The femtosecond mid-IR laser beam coming from the right side in the figure, is joined by a low power continuous-wave (CW) InGaAsP diode laser beam at a wavelength of 1.5 µm. This tracking beam is mainly used for alignment, as the near-IR or visible light cannot be used for tracking or imaging through the silicon substrates. After the alignment at the Si plate placed at the Brewster angle ($\theta_B = 74°$), both beams are collimated and directed into an objective lens and focused onto the substrate, shown on the left side in the figure. The objective lens mounted on a vertical stationary optical bench is a reflective type microscope objective, which has no chromatic aberration at different wavelengths so that the two laser beams can have the same focus at the substrate surface.

The silicon substrate is mounted on top of a manual Z stage to adjust the focal depth of the laser beam into the substrate. Below the Z stage is a manually adjustable tip & tilt stage, which is used to level the substrate to ensure that the laser focus stays the same across the full substrate during the movement. A motorized X-Y translation stage from Aerotech sits at the bottom, and it is controlled by a program built in C# to carry out the horizontal motion of the substrate. An InGaAs SWIR Camera from FLIR, sensitive to the range 0.9–1.7µm, is mounted also on the vertical optical bench to the right side of the beamsplitter, to observe and find the focus at the surface of the silicon substrate.

In our experiments, we first use only the tracking beam to focus on the thermally oxidized silicon wafers. Then we turn on the femtosecond laser beam to start the micromaching, and implement the movement program of the XY stage according to the machining pattern, which will be discussed in more detail in the next section. Reflected surface wavefronts from the substrate are measured with a Zygo interferometer before and after the micromachining, to deduce the change in the surface profile of the silicon wafer. This change can be used to reconstruct a surface height change map through fitting to a set of basis functions such as Zernike polynomials, and to calculate the stress distribution across the substrate caused by the micromachining process.

2.3 Micromachining pattern

The term micromachining pattern refers to the distribution of the laser shots on the whole substrate, which is related to how much stress to add or remove locally in smaller regions on the wafer. For a real X-ray mirror with different amount of figure errors across the whole surface, a non-uniform machining pattern is needed to precisely match the variation of the error distribution in different regions. In order to do this, we have to characterize the amount of stress created by this micromachining process as a function of various parameters, such as pulse energy, machining density, number of laser shots per spot, etc.

In principle we would like to study how an individual laser shot affects the stress distribution in the substrate, but this effect is almost negligible to the metrology tool. As a proof of concept, we can calibrate this effect by applying a uniform micromachining pattern across the full wafer and then measure the average change of

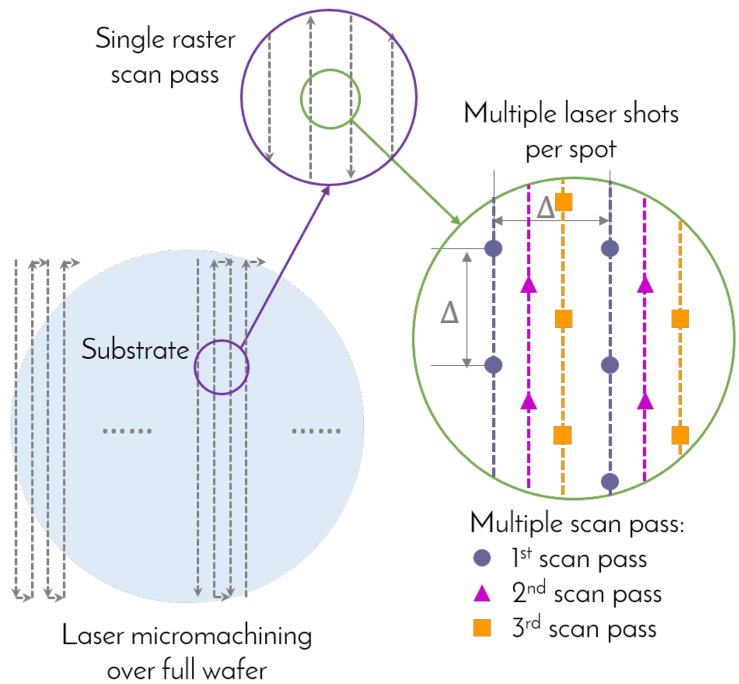

Figure 3: Illustration of the uniform micromachining pattern across a full wafer with multi-pass correction (top down view).

curvature. A simple way is to create some equally spaced features, i.e., micromachine holes with the same separation in both X and Y direction on the entire wafer. The illustration of this pattern is shown in Figure 3.

The basic machining path is a raster scan over a square region (100 mm × 100 mm) covering the entire wafer. The stage with the substrate moves in the horizontal plane at a constant velocity (50 mm/s). After every $\Delta = 500\,\mu\text{m}$ (Δ is the machining interval), the stage pauses its motion and dwells at the same position for 50 ms, so that the laser beam can shoot 50 laser shots into the same spot to drill a deep hole. In the enlarged picture of Figure 3, the round dark grey dots connected by dotted lines represent this raster dwell scan pass.

Furthermore, one of the advantage of this method is its capability of multi-pass corrections. To demonstrate this, after measuring the surface profile of the wafer after one micromachining scan pass, we put the same wafer back on stage and scan it again, with the same micromachining scan pass but offset by a small distance from the first pass. We can keep adding more scanning passes as long as there is still enough unmachined space on the wafer. The drawing in Figure 3 shows three different scan passes, where the magenta triangles and the orange squares represent the second and third micromachining scan passes. Therefore, the density of the micromachined holes increases linearly according to $\frac{p}{\Delta^2}$, where p is the number of the scanning passes ranging from 0 to 3, and the total materials removed also increase proportionally with the number of total scans.

3. RESULTS

In this section we present some initial experimental results from flat silicon wafers after micromachining according to the aforementioned scan patterns. There are two types of wafers used, both of which are 100 mm in diameter and 525 µm thick. The difference is in the thickness of the thermal oxide layer: one of them is 1 µm thick and for the other type it is only 50 nm.

3.1 Images of the micromachined holes

First we present the micromachining results from sample Si2019072102 with 1 µm–thick thermal oxide layer. It is machined with three scan passes according to the pattern illustrated in Figure 3, all of which have the same machining parameters: 25 µJ pulse energy, 500 µm machining interval and 50 laser shots per dot. Each machining pass takes nearly 2 h to finish, with a lot of the time spent on the acceleration and deceleration of the stage.

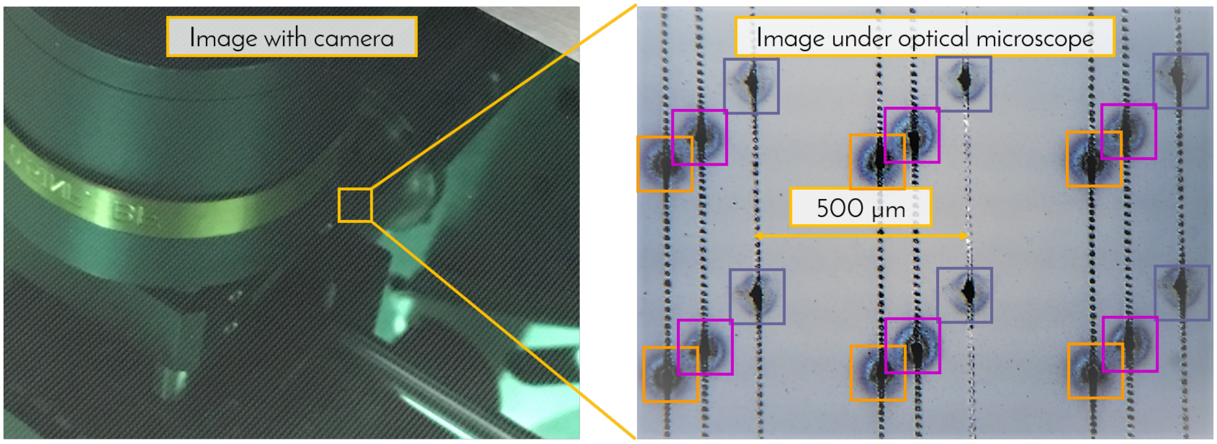

Figure 4: Photographs of silicon sample Si2019072102 after three micromachining passes. Left: Image of the substrate surface taken with a camera while the sample still sits on the stage. Right: Enlarged area of the surface seen with an optical microscope, showing three micromachining passes labeled in boxes of different colors.

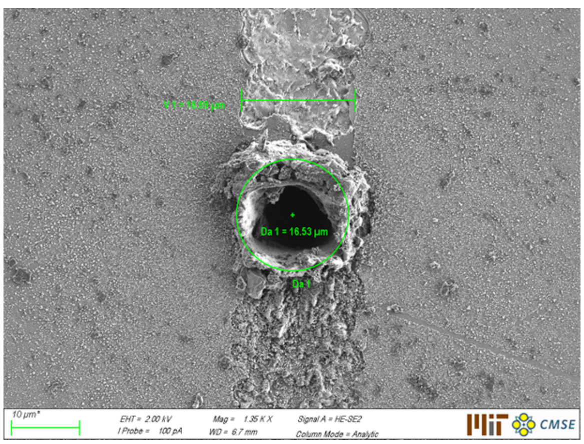

(a) Surface image: Width of a typical hole is about 17±2 µm.

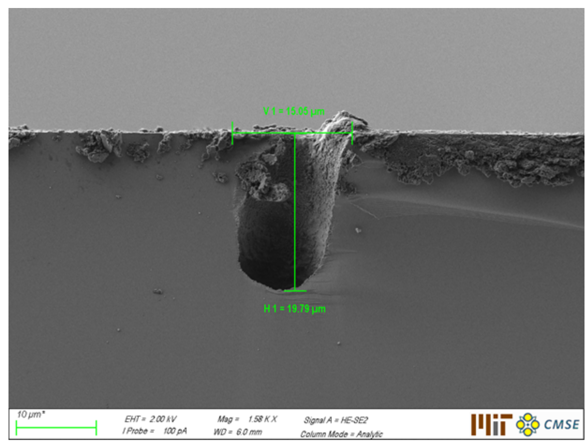

(b) Cross-section image: Depth of a typical hole after exposure to 50 laser shots is about 20 µm.

Figure 5: SEM images showing the width and depth of the targeted micromachined holes.

Figure 4 shows the photographs of this sample after all three micromachining passes. The picture on the left is taken with a camera while the sample is still mounted on the stage, and the reflection of the objective lens from the wafer surface can be easily seen. The less reflective white dots on the surface are the targeted micromachined holes. The picture on the right is taken with an optical microscope of this surface over a much smaller region. The circular areas labeled in colored boxes in this picture are the targeted machined spots exposed to multiple laser shots, while the dotted lines connecting them show the scan passes. This is because the laser keeps pulsing at its repetition frequency when the sample is moving, so each laser pulse hits a different spot on the wafer and some surface material is removed by these pulses as well. The ring-shaped shadows outside the circular targeted machined spots may come from the strains in the surrounding regions, but the exact reasons are still to be investigated. The different colors of the boxes indicate different machining passes, and they follow the same color scheme used in Figure 3. In the picture we can also see that the separation of spots in one machining pass is 500 µm, as labeled in the picture, and the offsets between two machining passes is about 100 µm.

Scanning electron microscopy (SEM) is used to examine these targeted micromachined areas in closer detail. Figure 5 shows two images taken with a Zeiss SEM. (a) is a surface image of the sample viewed from the top, at the center of which is a hole drilled by 50 laser pulses, showing a diameter of about 17 µm. The lightly modified areas above and beneath the hole come from the single pulse micromachining when the sample is moving relative to the laser beam. (b) shows a cross-section image of the cleaved sample viewed from the side. The image not only reveals the depth of the hole after been exposed to 50 laser shots to be 20 µm, but also shows very clean edges with no microcracks into the surrounding material. This is an important aspect for the robustness and stability of the telescope mirrors.

3.2 Measurements of wafer deformation

As stated before, mirror surface topography is measured with a Zygo interferometer before and after each micromachining pass, and the change in the surface profile is reconstructed by fitting to Zernike polynomials. The first three rows in Figure 6 exhibit the cumulative changes of the surface profiles in two samples after three micromachining passes, i.e., the figures in each row were obtained by subtracting the initial surface measurement of the raw sample from the measurement after the corresponding machining pass. The surface peak-to-valley (P-V) value is also listed on top of each figure, and smallest P-V change is less than 0.5 µm over the entire wafer, which shows good machining resolution.

The left column is from sample Si2019072102 which has 1 µm–thick thermal oxide layer, and the right column is from sample Si2019080101 with a thermal oxide layer of only 50 nm. Everything else is the same for the two samples, and they were machined in the exact same way. In both cases, a bowl shape deformation is detected, which gets deepened as the number of machining pass increases. It is clear from these figures that the femtosecond laser micromachining has created bending moments on the silicon wafers to create such bowl-shaped deformations. It is also worth noticing that the sample with thinner thermal oxide layer bends less than the one with thicker oxide.

3.3 Calculation of the integrated stress

Integrated film stress refers to the stress in the film integrated over its thickness, also equivalent to the mean film stress multiplied by the film thickness. It is an important concept for stress compensation, and knowing how much stress can be created from a uniform micromachining scanning pattern is the first step to correct a real mirror. A stress map to compensate for can be informed from the initial figure errors of the mirror, and a non-uniform scanning pattern needs to be implemented to neutralize these stress distributions, similar to the method used for ion implantation.[25]

In our experiments, after obtaining the difference map of the substrate surface profile before and after each micromachining pass, we can derive the surface curvature from the fitting. Then the integrated stress in two directions X and Y can be calculated by employing Stoney's equation:[26]

$$S_{xx} = \frac{E_s h_s^2}{6(1-\nu_s^2)}(\kappa_{xx} + \nu_s \kappa_{yy}) \tag{1}$$

$$S_{yy} = \frac{E_s h_s^2}{6(1-\nu_s^2)}(\nu_s \kappa_{xx} + \kappa_{yy}) \tag{2}$$

where E_s, ν_s are the Young's modulus and Poisson's ratio of the substrate, h_s is the substrate thickness, and κ_{xx}, κ_{yy} are the curvatures in X and Y directions. This calculation results in a stress map over the whole surface. Since we have uniform patterning over the whole wafer, the mean value of each stress term is used in the following analysis without loss of generality.

The integrated stress of the aforementioned two samples is shown in the last row of Figure 6, where the orange color represents S_{xx} and the blue is S_{yy}. The horizontal axis is the fraction of area removed, which is simply defined as the total area of the micromachined holes over the area of the entire wafer. It is also proportional to the micromachining density assuming all the holes are of the same size, as well as the number of micromachining passes since they all have the same machining pattern. The vertical axis represents the integrated stress with

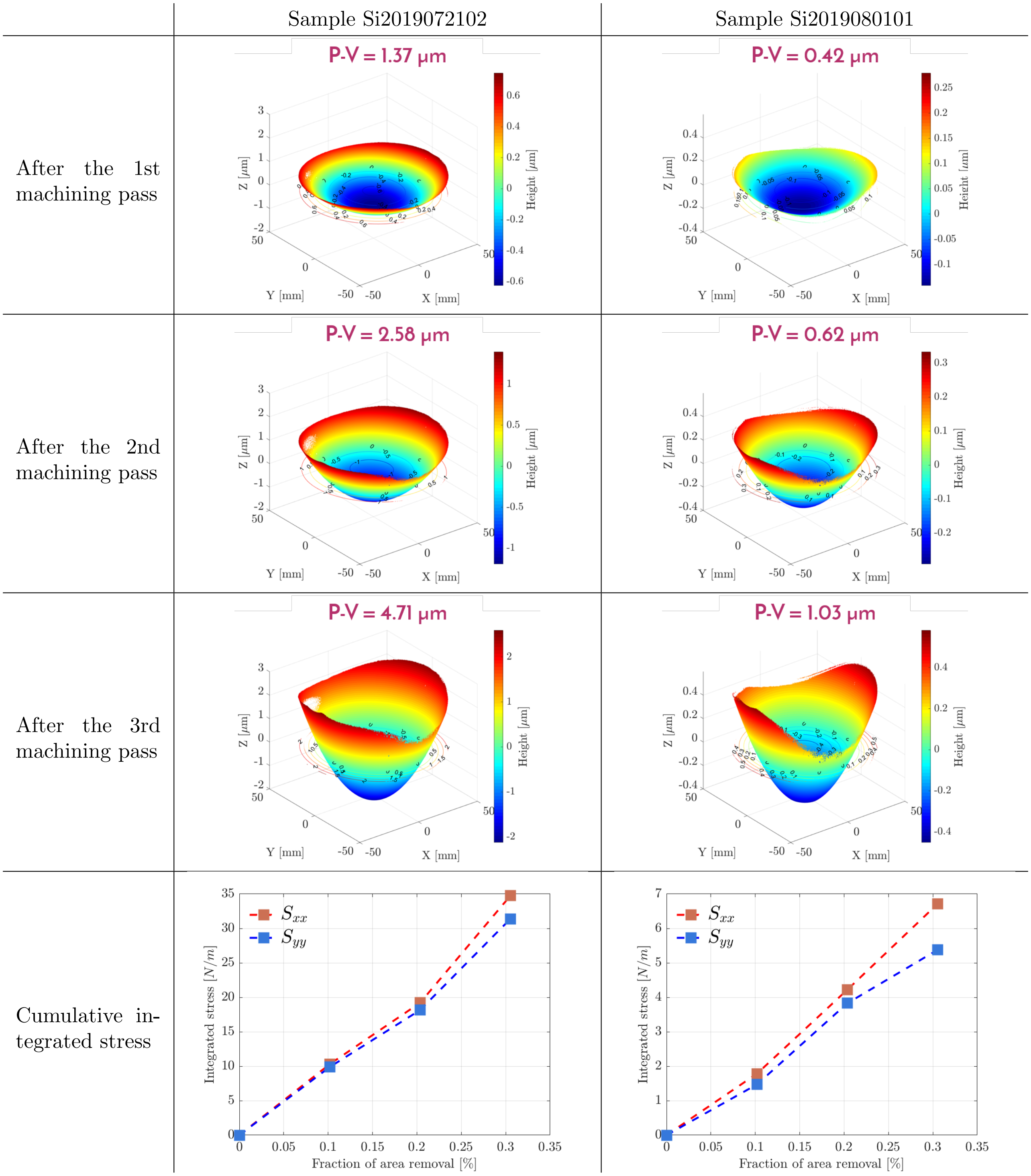

Figure 6: Measured cumulative changes of the surface profiles in two samples Si2019072102 (left column) and Si2019080101 (right column) after three micromachining passes (first three rows), as well as the cumulative integrated stress (last row).

units of [N/m]. Note that the intrinsic stress in thermal oxides is around 300 MPa, so the original integrated stress in a 1 µm thick thermal oxide layer is 300 N/m.

The important messages from these figures are:

- The two stress components in different directions are very close in magnitude to each other, indicating that the stress generated from this process is equal-biaxial stress;
- The sign of the stress is positive, meaning that we have removed some compressive stress from the original thermal oxide layer, which is also equivalent to adding a new layer of tensile stress onto the back of the substrate;
- The amount of induced stress increases almost linearly with fraction of area removal, which suggests the possibility of correcting mirrors by varying the fraction of area removal in different regions;
- The stress compensation of this process if very effective, as it can remove 10 % ($= \frac{30\,\mathrm{N/m}}{300\,\mathrm{N/m}}$) of the intrinsic compressive stress with the removal of only 0.3 % of the thermal oxide.

We speculate that the effectiveness of this method, that very little oxide removal can lead to great film stress change, may come from the fact that the femtosecond laser can drill small holes deep into the silicon substrates. Yet, some modeling and stress analysis is required to prove this speculation. Figure 7 compares the stress removal in the two samples of different oxide layer thickness, and it shows that the integrated stress is only five times smaller for the sample with 50 nm thermal oxide layer than the one with 1 µm thermal oxide, despite 20 times thinner film. This demonstrates that the stress removal of the thermal oxide film using this process is closely associated with the film thickness, and we may perform mirror corrections by growing proper thickness of thermal oxide depending on the stress needed.

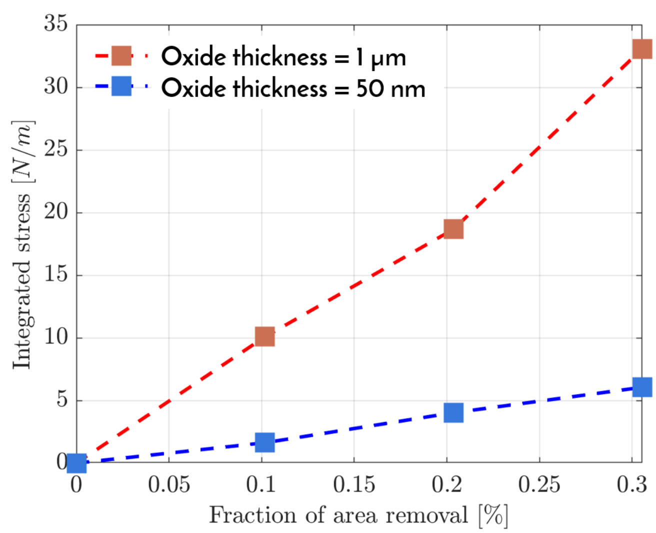

Figure 7: Comparison of stress removal effect in the two samples of different oxide layer thickness.

4. SUMMARY

In conclusion, we have developed a new method using femtosecond laser micromachining with thermal oxide patterning for correction of figure errors in thin mirrors. We have designed an optical system and built a new tool for micromachining flat silicon wafers. We have measured surface deformation from uniform micromachining patterns with an interferometer, and calculated the stress distribution in the substrate from this process. We showed that femtosecond laser micromachining provides an effective way to remove the intrinsic compressive stress in the thermal oxide layer, and it can achieve a reduction of 10 % in the stress with the removal of only

0.3 % of thermal oxide. Finally, we demonstrated the potential for correcting mirrors by using the appropriate micromachining parameters such fractional area removal in different regions of the mirror substrates.

Nevertheless, more studies are needed to explore the influences of various micromachining parameters. Strength tests and stability tests are required to prove that the micromachined mirrors will survive the space environment. A finite element model will be desired to analyze the stress removal around micromachined regions. Furthermore, to demonstrate the correction of an actual X-ray mirror, a correction algorithm based on the surface error map needs to be built. Currently, we are working on building a more advanced micromachining system with a new stage to perform non-uniform scanning patterns. It is our belief that with a better stage and faster laser, femtosecond laser micromachining can correct thin mirrors with high accuracy in just minutes, which is very promising for future X-ray telescope missions.

ACKNOWLEDGMENTS

This work has been supported by NASA APRA grants NNX16AD01G and NNX17AE47G. The laser is supported by US DOD Office of Navy Research (ONR) DURIP (N00014-17-1-2744). The authors give special thanks to members of MIT SNL for valuable discussions, and to MIT RLE and CMSE for facilities support.

REFERENCES

[1] O'Dell, S. L., Allured, R., Ames, A. O., Biskach, M. P., Broadway, D. M., Bruni, R. J., Burrows, D. N., Cao, J., Chalifoux, B. D., Chan, K.-W., et al., "Toward large-area sub-arcsecond X-ray telescopes II," in [*Adaptive X-Ray Optics IV*], **9965**, 996507, International Society for Optics and Photonics (2016).

[2] Zhang, W. W., "Manufacture of mirror glass substrates for the NuSTAR mission," in [*SPIE Optical Engineering+ Applications*], 74370N, International Society for Optics and Photonics (2009).

[3] Zuo, H. E., Yao, Y., Chalifoux, B. D., DeTienne, M. D., Heilmann, R. K., and Schattenburg, M. L., "Recent progress on air-bearing slumping of segmented thin-shell mirrors for X-ray telescopes: experiments and numerical analysis," in [*Optics for EUV, X-Ray, and Gamma-Ray Astronomy VIII*], **10399**, 1039910, International Society for Optics and Photonics (2017).

[4] Kilaru, K., Ramsey, B. D., Baumgartner, W. H., Bongiorno, S. D., Broadway, D. M., Champey, P. R., Davis, J. M., O'Dell, S. L., Elsner, R. F., Gaskin, J. A., et al., "Full-shell X-ray optics development at nasa marshall space flight center," *Journal of Astronomical Telescopes, Instruments, and Systems* **5**(2), 021010 (2019).

[5] Collon, M. J., Vacanti, G., Barrière, N. M., Landgraf, B., Guenther, R., Vervest, M., Voruz, L., Verhoex, S., Babić, L., van der Hoeven, R., et al., "Silicon pore optics mirror module production and testing," in [*International Conference on Space OpticsICSO 2018*], **11180**, 1118023, International Society for Optics and Photonics (2019).

[6] Zhang, W. W., Allgood, K. D., Biskach, M. P., Chan, K.-W., Hlinka, M., Kearney, J. D., Mazzarella, J. R., McClelland, R. S., Numata, A., Olsen, L. G., et al., "Monocrystalline silicon and the meta-shell approach to building X-ray astronomical optics," in [*Optics for EUV, X-Ray, and Gamma-Ray Astronomy VIII*], **10399**, 103990S, International Society for Optics and Photonics (2017).

[7] Riveros, R. E., Biskach, M. P., Allgood, K. D., Kearney, J. D., Hlinka, M., Numata, A., and Zhang, W. W., "Fabrication of lightweight silicon X-ray mirrors for high-resolution X-ray optics," in [*Space Telescopes and Instrumentation 2018: Ultraviolet to Gamma Ray*], **10699**, 106990P, International Society for Optics and Photonics (2018).

[8] Zhang, W. W., Allgood, K. D., Biskach, M. P., Chan, K.-W., Hlinka, M., Kearney, J. D., Mazzarella, J. R., McClelland, R. S., Numata, A., Riveros, R. E., et al., "Astronomical X-ray optics using monocrystalline silicon: high resolution, light weight, and low cost," in [*Space Telescopes and Instrumentation 2018: Ultraviolet to Gamma Ray*], **10699**, 106990O, International Society for Optics and Photonics (2018).

[9] Walker, J., Liu, T., Tendulkar, M., Burrows, D., DeRoo, C., Allured, R., Hertz, E., Cotroneo, V., Reid, P., Schwartz, E., et al., "Design and fabrication of adjustable X-ray optics using piezoelectric thin films," in [*Optics for EUV, X-Ray, and Gamma-Ray Astronomy VIII*], **10399**, 103991K, International Society for Optics and Photonics (2017).

[10] Chalifoux, B. D., Yao, Y., Woller, K. B., Heilmann, R. K., and Schattenburg, M. L., "Compensating film stress in thin silicon substrates using ion implantation," *Optics Express* **27**(8), 11182–11195 (2019).

[11] Yao, Y., Chalifoux, B. D., Heilmann, R. K., and Schattenburg, M. L., "Thermal oxide patterning method for compensating coating stress in silicon substrates," *Optics Express* **27**(2), 1010–1024 (2019).

[12] Davis, K. M., Miura, K., Sugimoto, N., and Hirao, K., "Writing waveguides in glass with a femtosecond laser," *Optics Letters* **21**(21), 1729–1731 (1996).

[13] Dausinger, F., Lichtner, F., and Lubatschowski, H., [*Femtosecond technology for technical and medical applications*], vol. 96, Springer Science & Business Media (2004).

[14] Osellame, R., Cerullo, G., and Ramponi, R., [*Femtosecond laser micromachining: photonic and microfluidic devices in transparent materials*], vol. 123, Springer Science & Business Media (2012).

[15] Gattass, R. R. and Mazur, E., "Femtosecond laser micromachining in transparent materials," *Nature Photonics* **2**(4), 219–225 (2008).

[16] Liu, X., Du, D., and Mourou, G., "Laser ablation and micromachining with ultrashort laser pulses," *IEEE Journal of Quantum Electronics* **33**(10), 1706–1716 (1997).

[17] Stuart, B. C., Feit, M. D., Herman, S., Rubenchik, A., Shore, B., and Perry, M., "Nanosecond-to-femtosecond laser-induced breakdown in dielectrics," *Physical Review B* **53**(4), 1749 (1996).

[18] Chichkov, B. N., Momma, C., Nolte, S., Von Alvensleben, F., and Tünnermann, A., "Femtosecond, picosecond and nanosecond laser ablation of solids," *Applied Physics A* **63**(2), 109–115 (1996).

[19] Sundaram, S. and Mazur, E., "Inducing and probing non-thermal transitions in semiconductors using femtosecond laser pulses," *Nature Materials* **1**(4), 217 (2002).

[20] Nolte, S., Will, M., Burghoff, J., and Tuennermann, A., "Femtosecond waveguide writing: a new avenue to three-dimensional integrated optics," *Applied Physics A* **77**(1), 109–111 (2003).

[21] Zuo, H. E., Chalifoux, B. D., Heilmann, R. K., and Schattenburg, M. L., "Ultrafast laser micro-stressing for correction of thin fused silica optics for the Lynx X-ray telescope mission," in [*Space Telescopes and Instrumentation 2018: Ultraviolet to Gamma Ray*], **10699**, 1069954, International Society for Optics and Photonics (2018).

[22] Kobeda, E. and Irene, E., "Intrinsic SiO2 film stress measurements on thermally oxidized Si," *Journal of Vacuum Science & Technology B: Microelectronics Processing and Phenomena* **5**(1), 15–19 (1987).

[23] Fitch, J., Bjorkman, C., Lucovsky, G., Pollak, F., and Yin, X., "Intrinsic stress and stress gradients at the SiO2/Si interface in structures prepared by thermal oxidation of Si and subjected to rapid thermal annealing," *Journal of Vacuum Science & Technology B: Microelectronics Processing and Phenomena* **7**(4), 775–781 (1989).

[24] Chan, K.-W., Zhang, W. W., Windt, D., Hong, M.-L., Saha, T., McClelland, R., Sharpe, M., and Dwivedi, V. H., "Reflective coating for lightweight X-ray optics," in [*Space Telescopes and Instrumentation 2012: Ultraviolet to Gamma Ray*], **8443**, 84433S, International Society for Optics and Photonics (2012).

[25] Chalifoux, B., Yao, Y., Zuo, H. E., Heilmann, R. K., and Schattenburg, M. L., "Compensating film stress in silicon substrates for the Lynx x-ray telescope mission concept using ion implantation," in [*Space Telescopes and Instrumentation 2018: Ultraviolet to Gamma Ray*], **10699**, 1069959, International Society for Optics and Photonics (2018).

[26] Freund, L. B. and Suresh, S., [*Thin film materials: stress, defect formation and surface evolution*], Cambridge University Press (2004).